Journal of Coordination Chemistry

ISSN: 0095-8972 (Print) 1029-0389 (Online) Journal homepage: http://www.tandfonline.com/loi/gcoo20

Two pillared-helical-layer frameworks based on spiral chainlike metavanadate and $[M(btx)]^{2+}$ complexes

Zhigang Liu, Wen Qi, Chunyan Li, Yanfei Qi, Juan Li, Enbo Wang & Xiaoyu Yang

To cite this article: Zhigang Liu, Wen Qi, Chunyan Li, Yanfei Qi, Juan Li, Enbo Wang & Xiaoyu Yang (2015) Two pillared-helical-layer frameworks based on spiral chainlike metavanadate and $[M(btx)]^{2+}$ complexes, Journal of Coordination Chemistry, 68:5, 743-751, DOI: 10.1080/00958972.2014.1003050

To link to this article: http://dx.doi.org/10.1080/00958972.2014.1003050

Journal of Coordination Chemistry, 2015
Vol. 68, No. 5, 743–751, http://dx.doi.org/10.1080/00958972.2014.1003050

Two pillared-helical-layer frameworks based on spiral chainlike metavanadate and $[M(btx)]^{2+}$ complexes

ZHIGANG LIU†, WEN QI†, CHUNYAN LI†, YANFEI QI*†, JUAN LI†, ENBO WANG‡ and XIAOYU YANG†

†The 3rd Hospital, School of Public Health, Jilin University, Changchun, PR China
‡Key Laboratory of Polyoxometalates Science of Ministry of Education, Department of Chemistry, Northeast Normal University, Changchun, PR China

(*Received 19 August 2014; accepted 11 December 2014*)

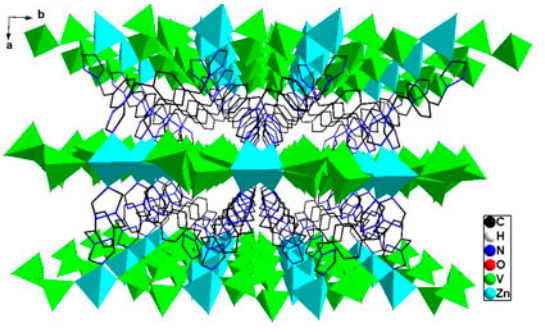

Two new organic–inorganic hybrids are composed of $\{M'V_2O_6\}$ bimetallic oxide layers pillared by the interlamellar btx ligands, containing novel $[V_2O_6]^{2-}$ and $\{M(btx)\}^{2+}$ meso-helixes.

Two new isomorphous oxovanadium composite solids, $[Zn(btx)V_2O_6]$ (**1**) and $[Cu(btx)V_2O_6]$ (**2**) (btx = 1,4-bis(triazol-1-ylmethyl)benzene), have been synthesized and characterized by elemental analysis, IR, TGA, and single-crystal X-ray diffraction. The structures of **1** and **2** are composed of $\{MV_2O_6\}$ (M = Zn or Cu) bimetallic oxide layers, linked through $\{MO_2N_2\}$ building blocks and btx ligands into 3-D architectures. The two compounds consist of infinite spiral chains and all helical chains are meso-helices, which lead to racemic solid-state compounds. The electrochemical properties of the two compounds have been studied.

Keywords: Polyoxovanadates; Helix; Organic–inorganic hybrid; Electrochemical property

1. Introduction

The rational design of pillar-layered architectures, which have been proven to be an effective and controllable route to 3-D frameworks with large channels, received attention

*Corresponding author. Email: qiyanfei@jlu.edu.cn

because of their distinct structural feature of changeable pillaring fragments in the interlamellar regions [1, 2]. Compared to traditional methods, this strategy can effectively prevent the occurrence of lattice interpenetration, and porous frameworks can stabilize the functional groups by isolating their specific positions. In addition, immobilization of functional groups into porous hosts can enhance their functionalities [3, 4].

Polyoxovanadate, known for applications in catalysis, biology, and magnetism, are an outstanding class of functional secondary building blocks for construction of interesting functional porous materials [5–9]. Some suitable polyoxovanadate clusters have been utilized to generate 3-D materials [10–12]. The structural variety of polyoxovanadate, derived from the multiple oxidation states (III, IV, and V) and coordination geometries (tetrahedral, square pyramidal, and octahedral) of vanadium oxygen anions, makes it possible to fine-tune the redox potentials, acidities, and reactivities of polyoxovanadate-based functional porous materials [13–16]. Furthermore, polyoxovanadate in contrast to polymolybdate and polytungstate can form more flexible chain metavanadates to layered oxides and compact polyanions in hydrothermal conditions. Therefore, they can become important choices in constructing functional–pillared helical-layer frameworks, which may induce chirality [17, 18]. Chiral porous POM-based frameworks with potential applications in heterogeneous asymmetric catalysis and enantioselective separations have received extensive attention. Prominent work has been performed by the groups of Pope, Hill, Yamase and Kortz [19–24]. Recently, our group obtained two chiral POM-based 3-D architectures from $[BW_{12}O_{40}]^{5-}$ clusters and $[MnMo_9O_{32}]^{6-}$ chiral clusters, respectively [25]. The thermally more stable POM backbone can enhance the stability of the frameworks, which is an important issue that porous materials designers encounter. According to the above considerations, our current synthetic strategy is to acquire 3-D porous frameworks via 3d metal–organic coordination polymers and polyovanadate.

Judicious selection of ligands is very important because deliberate structural changes of organic building blocks such as length, flexibility, and symmetry can dramatically change the final structural motifs. Recently, there is interest in the linear flexible N,N′-bridging ligands, for instance derivatives of imidazole and 1,2,4-triazole [26]. Our attention is attracted by 1,4-bis(triazol-1-ylmethyl)benzene (btx) (figure S1, see online supplemental material at http://dx.doi.org/10.1080/00958972.2014.1003050), which are flexible and can connect various metal ions forming multi-dimensional coordination polymers. By incorporation of btx into the polyvanadate framework via hydrothermal technology, we isolated two isomorphous organic–inorganic hybrids, $[Zn(btx)V_2O_6]$ (**1**) and $[Cu(btx)V_2O_6]$ (**2**), which are composed of $\{M'V_2O_6\}$ bimetallic oxide layers pillared by interlamellar btx ligands, containing $[V_2O_6]^{2-}$ and $\{M(btx)\}^{2+}$ meso-helixes. Although a large variety of organic–inorganic $\{M_xL_yVO\}$ hybrid materials have been isolated, the 3-D framework containing pillared helical-layer structure is still rare.

2. Experimental

2.1. *General procedures*

All chemicals were commercially purchased and used without purification. Elemental analyses (C, H, and N) were performed on a Perkin-Elmer 2400 CHN Elemental Analyzer. Zn and V were determined by a Leaman inductively coupled plasma spectrometer. IR spectra were recorded from 400 to 4000 cm^{-1} on an Alpha Centaurt FT/IR spectrophotometer using KBr pellets. TG analyses were performed on a Perkin-Elmer TGA7 instrument in flowing

N_2 with a heating rate of 10 °C min^{-1}. A CHI 660 Electrochemical Workstation connected to a Digital-586 personal computer was used for control of the electrochemical measurements and for data collection. A conventional three-electrode system was used. The working electrodes were **1** and **2** bulk-modified carbon paste electrode (**1**-CPE and **2**-CPE). A SCE was used as a reference electrode and Pt gauze as a counter electrode.

2.2. *Synthesis of [Zn(btx)V_2O_6] (1)*

A mixture of $NaVO_3$ (0.3 mM), $Zn(NO_3)_2{\cdot}6H_2O$ (0.1 mM), btx (0.1 mM), four drops of Et_3 N/CH_3CN mixture (1:9), CH_3CN (1 mL) and H_2O (9 mL) was placed in a Parr Teflon-lined stainless steel vessel (15 mL), and then the vessel was sealed and heated at 120 °C for 3 days. After the mixture was slowly cooled to room temperature, pale-yellow crystals of **1** were obtained (yield: 53% based on V). Anal. Calcd for $C_{12}H_{12}N_6O_6ZnV_2$: C, 28.62; H, 2.40; N, 16.69; V, 20.23; Zn, 12.98%. Found: C, 28.60; H, 2.75; N, 16.68; V, 20.11; Zn, 12.88%. IR spectrum (cm^{-1}): 3436(m), 3127(m), 3099(m), 3040(w), 2924(w), 2854(w), 1929(w), 1641(w), 1534(s), 1484(w), 1421(s), 1371(w), 1344(w), 1302(w), 1279(s), 1225 (vs), 1183(w), 1136(s), 1018(s), 1004(s), 971(s), 917(vm), 892(m), 869(vm), 827(m), 794 (s), 749(vm), 670(m), 635(s), 494 (w).

2.3. *Synthesis of [Cu(btx)V_2O_6] (2)*

The same procedure for preparing **1** was used, except that $Cu(NO_3)_2{\cdot}6H_2O$ (0.1 mM) was used instead of $Zn(NO_3)_2{\cdot}6H_2O$ (35% yield based on V). After slowly cooling the bomb to room temperature, the resulting pale-blue crystals of **2** were collected as a pure phase from the mother liquid. The crystals were washed with distilled water and dried at ambient temperature. Anal. Calcd $C_{12}H_{12}N_6O_6CuV_2$: C, 28.73; H, 2.41; N, 16.75; Cu, 12.67; V, 20.31%. Found: C, 28.67; H, 2.76; N, 16.71; Cu, 12.65; V, 20.28%. IR spectrum (cm^{-1}): 3440(m), 3127(m), 3101(m), 3041(w), 1929(w), 1606(w), 1534(s), 1484(w), 1428(s), 1371 (w), 1348(w), 1279(s), 1225(vs), 1183(w), 1135(s), 1017(s), 1003(s), 971(s), 892(m), 869 (vm), 827(m), 787(s), 749(vm), 671(m), 637(s), 496 (w).

2.4. *X-ray crystallography*

The structures of **1** and **2** were determined by single crystal X-ray diffraction. Data were collected on a Rigaku R-AXIS RAPID IP diffractometer with Mo-Kα (λ = 0.71073 Å) radiation at 293 K. Empirical absorption corrections (ψ scan) were applied for **1** and **2**. The structures were solved by the direct method and refined by full-matrix least squares on F^2 using the SHELXL-97 software [20]. All nonhydrogen atoms were refined anisotropically. Hydrogens of organic ligands were fixed in ideal positions. A summary of crystal data and structure refinements for **1** and **2** is provided in table 1. Selected bond lengths and angles are listed in table 2.

3. Results and discussion

3.1. *Structure description*

Single-crystal X-ray diffraction analyses revealed that the structures of the isomorphous materials [M(btx)V_2O_6] (M = Zn (**1**) and Cu (**2**)) consist of {M′V_2O_6} bimetallic oxide

Table 1. Crystal data and structure refinements for **1** and **2**.

	1	**2**
Formula	$C_{12}H_{12}N_6O_6ZnV_2$	$C_{12}H_{12}N_6O_6CuV_2$
M_r	503.53	501.70
T [K]	293(2)	293(2)
Crystal system	Monoclinic	Monoclinic
Space group	$P2_1/c$	$P2_1/c$
a [Å]	19.494(4)	19.471(4)
b [Å]	8.2740(2)	8.2704(17)
c [Å]	10.561(2)	10.556(2)
α [°]	90	90
β [°]	97.88(3)	98.03(3)
γ [°]	90	90
V [Å^3]	1687.3(6)	1683.2(6)
Z	4	4
ρ_{calcd} [g cm^{-3}]	1.982	1.980
μ [mm^{-1}]	2.541	2.385
R_{int}	0.0982	0.1163
Data/parameters	2826/245	2959/244
Goodness of fit	1.0009	1.004
R_1[a] [$I > 2\sigma(I)$]	0.0623	0.0593
wR_2[b] [$I > 2\sigma(I)$]	0.1150	0.1322
Largest residuals [e Å^{-3}]	0.530/−0.709	0.678/−0.558

[a]$R_1 = \sum||F_0| - |F_C||/\sum|F_0|$.
[b]$wR_2 = \sum[w(F_0^2 - F_C^2)^2]/\sum[w(F_0^2)^2]^{1/2}$.

Table 2. Selected bond lengths [Å] for **1** and **2**.

Compound **1**			
V(1)–O(2)	1.610(4)	V(2)–O(5)	1.615(3)
V(1)–O(3)	1.696(4)	V(2)–O(6)#1	1.682(4)
V(1)–O(1)	1.786(4)	V(2)–O(4)	1.780(4)
V(1)–O(4)	1.796(3)	V(2)–O(1)#2	1.797(4)
Zn(1)–O(3)	1.930(4)	Zn(1)–N(4)	1.992(4)
Zn(1)–O(6)	1.948(4)	Zn(1)–N(1)	2.014(4)
Compound **2**			
V(1)–O(2)	1.596(4)	V(2)–O(5)	1.613(5)
V(1)–O(1)	1.688(4)	V(2)–O(4)	1.687(5)
V(1)–O(3)	1.781(5)	V(2)–O(6)#2	1.785(4)
V(1)–O(6)#1	1.795(4)	V(2)–O(3)	1.797(4)
Cu(1)–O(1)	1.930(4)	Cu(1)–O(4)#2	1.945(5)
Cu(1)–N(4)	2.006(5)	Cu(1)–N(1)	1.981(6)

for **1**: #1 x, $-y + 1/2$, $z - 1/2$; #2 x, $-y + 3/2$, $z - 1/2$; #3 x, $-y + 3/2$, $z + 1/2$; #4 x, $-y + 1/2$, $z + 1/2$; #5 $-x$, $-y + 1$, $-z + 2$; #6 $-x + 1$, $-y$, $-z + 2$; for **2**: #1 x, $y + 1$, z; #2 x, $-y + 3/2$, $z + 1/2$; #3 x, $y - 1$, z; #4 x, $-y + 3/2$, $z - 1/2$; #5 $-x + 1$, $-y$, $-z + 2$; #6 $-x$, $-y + 1$, $-z + 2$.

layers pillared by the interlamellar btx ligands. Here, the structure of $[Zn(btx)V_2O_6]$ is discussed. The oxide layers of **1** are constructed from $\{Zn(II)O_2N_2\}$ tetrahedra and $V(V)O_4$ tetrahedra. A noteworthy feature of **1** is the $[V_2O_6]^{2-}$ polyoxoanion chain. The VO_4 tetrahedra on the chain are joined with others by sharing corners to form an infinite meso-helix running along the c axis, as shown in figure 1. The meso-helix in **1** has a repetitive sequence of four-nuclear corner-sharing tetrahedra, V_4O_{12}, which is in a 2_1-screw processing manner. The corner-sharing VO_4 tetrahedral spiral chains are very rare. To our knowledge, only three compounds, $Ba(VO_3)_2$ [27], $Ni(en)_3(VO_3)_2$ [28], and H_3N

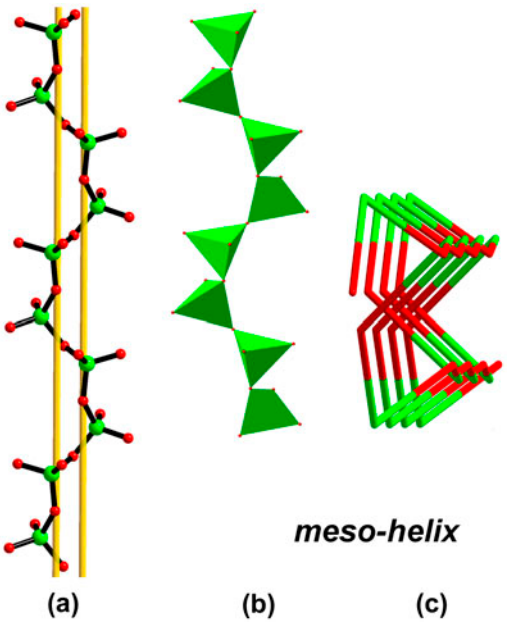

Figure 1. (a) Ball-stick, (b) Polyhedral, and (c) a simplified representation of the new eight-shaped helical $[V_2O_6]^{2-}$ chain of **1**.

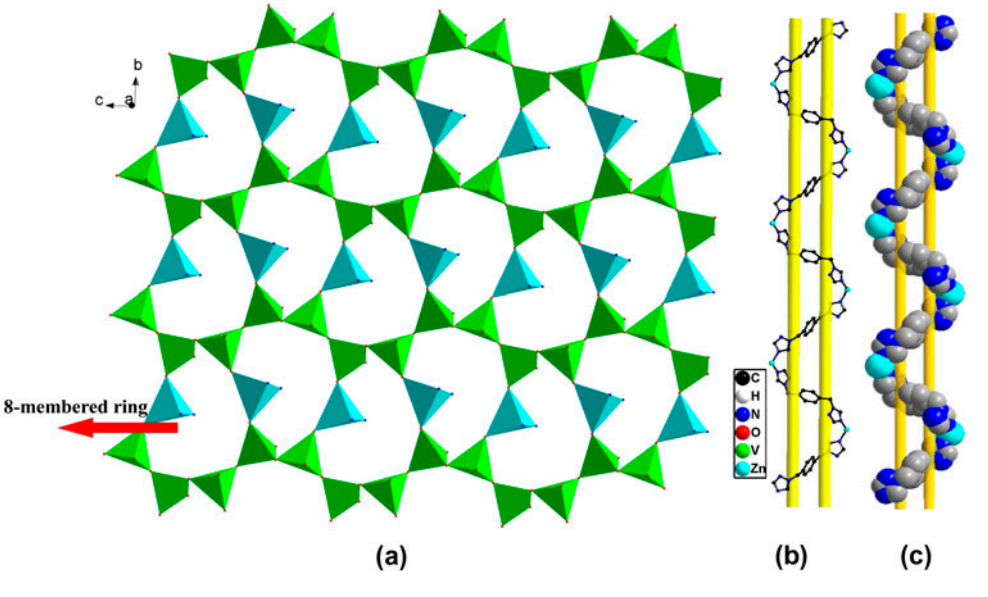

Figure 2. (a) View of the individual 2-D inorganic layer with eight-membered rings in **1** along the *a* axis, (b) ball-stick, and (c) space-filling views of the meso-helix of $\{Zn(btx)\}^{2+}$ in **1**.

$(CH_2)_4NH_3(VO_3)_2$ [29], have spiral-twisted chains. Therefore, **1** and **2** represent a new type of the twisted spiral $(VO_3)_\infty$ family.

There are two crystallographically independent vanadiums and one zinc in an asymmetric unit. The V(1) and V(2) sites possess tetrahedral geometry with one shorter terminal vanadyl bond (V1–O2 1.610(9) Å; V2–O5 1.614(2) Å) and three longer bonds (V1–O1 1.785 (2) Å; V1–O3 1.697(6) Å; V1–O4 1.792(5) Å; V2–O1 1.797(5) Å; V2–O4 1.783(2) Å; V2–O6 1.684(8) Å). The O–V–O angles are 70.92(9)°–157.99(1)°. Bond valence sum calculations give average values of 5.09 and 5.12 for V1 and V2, indicating that the V sites are in the +5 oxidation state in **1**. Each Zn(II) has four-coordinate tetrahedral geometry coordinated with oxo-groups from two different tetrahedral V sites on each of two adjacent chains (Zn1–O3 1.931(6) Å and Zn1–O6 1.946(4) Å) and two nitrogen donors from each of two btx ligands (Zn(1)–N4 1.989(3) Å and Zn(1)–N1 2.016(2) Å). The Zn(II) sites provide the connection between oxovanadate meso-helices to generate 2-D $\{ZnV_2O_6\}$ oxide substructure, as shown in figure 2(a). Within the 2-D layer, eight-membered rings $\{Zn_2V_6O_8\}$ are observed. The bimetallic oxide layer can be alternatively viewed as left- and right-handed helical chains constructed from $\{ZnO_2N_2\}$ and $\{VO_4\}$ building units, linked through V–O–V bonds. These single-stranded helical chains run along the crystallographic 2_1 axis in the *b* direction with a long pitch of 8.274(2) Å. There also is another meso-helix constructed from the Zn ions and linked by btx ligands in the structure of **1** [figure 2(b) and (c)]. In summary, as shown in figure 3, each bimetallic oxide layer is pillared face-to-face in a staggered manner with the flexible btx as the bridge.

3.2. *Synthesis consideration*

Hydrothermal reactions have proved to be effective for preparation of numerous solid-state oxides and organic–inorganic hybrid materials providing special reaction conditions in

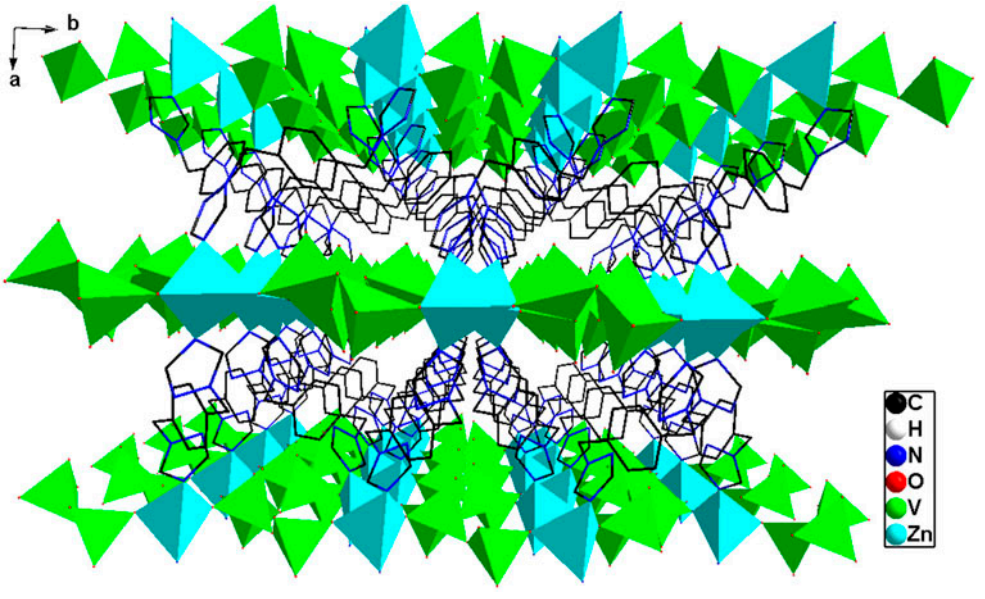

Figure 3. (a) Polyhedral and (b) schematic views of the 3-D–pillared layer framework down the *c* axis in **1**.

which different solubility problems are minimized. Hydrothermal conditions capture structurally more complicated metastable phases, intermediate phases, and special species. Herein, the new morphology oxovanadate $[V_2O_6]^{2-}$ is produced under hydrothermal conditions. In a specific hydrothermal process, many factors can affect the formation and crystal growth of products, such as the type of initial reactants, starting concentrations, pH values, reaction time, and temperature. The aqueous chemistry of vanadium compounds is very complex; it was anticipated that vanadate could form different building units in different pH ranges [30]. In our case, the pH of the reaction system was of crucial importance for crystallization of polyoxovanadate species. At pH 6.84, a new morphology oxovanadate $[V_2O_6]^{2-}$ was obtained.

Synthesis of more structurally interesting helix phases rather than the kinetic favored infinite straight chains remains a challenge. Helical chain is important to construct chiral structures. However, hydrothermal conditions are able to make the reaction shift from the thermodynamically to the kinetically stable product. It is important to reduce the crystallization speed of the infinite chain. The possible strategy is using mixed solvent H_2O/MeCN. The acetonitrile can reduce the precipitation of the metallic hydroxides and further hydrolysis of $[VO_3]^-$ species, or increase the solubilities of some intermediate M-ligand species. In **1** and **2**, the eight-shaped helix $\{Zn(btx)\}^{2+}$, $\{Cu(btx)\}^{2+}$, and $[V_2O_6]^{2-}$ were formed, which provided the pillared helical-layer based on POMs. In fact, the reaction of $[VO_3]^-$ with metal cationic species in organic solvents are sensitive to slight changes in the experimental conditions. It is very difficult to elucidate the mechanistic details on the formation of these species.

3.3. *FT-IR spectroscopy*

As shown in figures S2 and S3, peaks at 945, 818, 751, 724, 674, 639, 588, 543, 512, 457 cm^{-1}, **1**; 977, 969, 953, 939, 886, 834, 783, 768, 673, 657, 472 cm^{-1}, **2** are ascribed to vibrations of ν(V=O), ν(V–O–M) (M = V or Ag), respectively. The broad peak at 3430 cm^{-1} and the strong peak at 1640 cm^{-1} are attributed to lattice water in **1**. The strong bands at 3090, 2926, 1516, 1425, 1341, 1277, 1206, 1131, 1101 cm^{-1}, **1**; 3116, 2992, 1515, 1446, 1401, 1360, 1343, 1281, 1250, 1223, 1156, 1115, 1095, 1082 cm^{-1}, **2** are assigned to btx.

3.4. *Thermogravimetric analyses*

The TG curve of **1**, shown in figure S4, has the first weight loss at 233–276 °C; the second weight loss at 326–566 °C can be attributed to decomposition of btx. The whole weight loss 46.92% is in agreement with the calculated value 47.87%. The sample does not lose weight at temperatures higher than 600 °C. The remaining products are a mixture of ZnO and V_2O_5. Similar two weight loss curves are observed on the TGA curve of **2**, as shown in figure S5. The observed whole weight loss (49.27%) between 240 and 560 °C is consistent with the calculated value (48.04%). The remaining products are a mixture of CuO and V_2O_5.

3.5. *Electrochemical property*

Because vanadium oxides are of particular interest as candidates for active cathode materials in reversible lithium batteries or electrochemical devices, the electrochemical

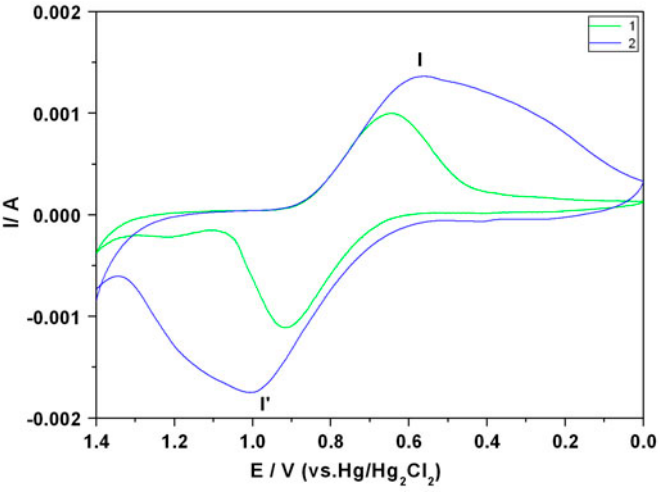

Figure 4. The cyclic voltammograms in 1 M H_2SO_4 at 10 mV s^{-1} scan rate for **1** (a) and **2** (b).

activities of **1** and **2** were investigated. To determine the redox properties of **1** and **2**, bulk-modified carbon paste electrode (**1**-CPE) was fabricated as the working electrode due to its insolubility in most solvents [31].

Figure 4 shows the voltammetric behavior of the working electrodes at 10 mV s^{-1} scan rate for **1** and **2** in 1 M H_2SO_4 aqueous solution. It can be seen that in the potential range 1150 to −1000 mV, two quasi-reversible redox peaks appear and the mean peak potentials $E_{1/2} = (E_{pa} + E_{pc})/2$ of the quasi-reversible redox peaks I–I′ are 0.775 V in **1** and 0.779 V in **2**, respectively. The waves I–I′ in the potential range may correspond to V(V)/V(IV) one-electron processes. The peak-to-peak separations between the corresponding anodic and cathodic peaks (ΔE_p) at the working electrode are larger than the reversible surface redox process, which might be due to nonideal behavior.

4. Conclusion

We have synthesized two new hybrids constructed from M(II)-complex subunits and low nuclear polyoxovanadate, $[V_2O_6]^{2-}$. Compared with high nuclear polyoxovanadate, the structures of low nuclear polyoxovanadate are more flexible and changeable. They can function as linkers, connectors, anion templates, and structure-directing agents to adjust the structure. Helix chain-like metavanadates can induce the formation of chiral structures. Although we did not get a chiral structure, the rare metavanadate meso-helix in **1** and **2** provides a strategy for synthesis of chiral-pillared helix-layer materials. The use of mixed solvent H_2O/MeCN reduces the crystallization speed and precipitation of metal hydroxides and further hydrolysis of $[VO_3]^-$ species increase the solubility of the intermediate M-ligand species and aid the formation of a helix structure. Further research in this subclass may concentrate on replacement of btx with other organic ligands and exploration of their attractive properties.

Supplemental material

Crystallographic data for the structural analyses have been deposited with the Cambridge Crystallographic Data Center, CCDC reference number 669340 for **1** and 669341 for **2**.

Funding

This work was financially supported by the NSFC [grant number 81402719], China Postdoctoral Science Foundation [grant number 20100481064], [grant number 2012T50307]; Young Scholars Program of Norman Bathune Health Science Center of Jilin University [grant number 2013202015]; Jilin Agricultural Product Quality and Safety Project [grant number 2011-Y11].

References

[1] R. Kitaura, G. Onoyama, H. Sakamoto, R. Matsuda, S. Noro, S. Kitagawa. *Angew. Chem., Int. Ed.*, **43**, 2684 (2004).
[2] C.Y. Su, A.M. Goforth, M.D. Smith, P.J. Pellechia, H.C. zur Loye. *J. Am. Chem. Soc.*, **126**, 3576 (2004).
[3] J. Lü, E.H. Shen, Y.G. Li, D.R. Xiao, E.B. Wang, L. Xu. *Cryst. Growth Des.*, **5**, 65 (2005).
[4] A.C. Sharma, A.S. Borovik. *J. Am. Chem. Soc.*, **122**, 8946 (2000).
[5] C.L. Hill. *Chem. Rev.*, **98**, 327 (1998).
[6] M.T. Pope, A. Müller. *Angew. Chem., Int. Ed. Engl.*, **30**, 34 (1991).
[7] Y. Kikukawa, S. Yamaguchi, K. Tsuchida, Y. Nakagawa, K. Uehara, K. Yamaguchi, N. Mizuno. *J. Am. Chem. Soc.*, **130**, 5472 (2008).
[8] D.L. Long, R. Tsunashima, L. Cronin. *Angew. Chem., Int. Ed.*, **49**, 1736 (2010).
[9] L. Cronin, A. Müller. *Chem. Soc. Rev.*, **41**, 7333 (2012).
[10] M.I. Khan, E. Yohannes, R.J. Doedens. *Angew. Chem. Int. Ed.*, **38**, 1292 (1999).
[11] A. Wutkowski, C. Näther, P. Kögerler, W. Bensch. *Inorg. Chem.*, **52**, 3280 (2013).
[12] Y.F. Qi, K. Xu, L.J. Lu, J. Li, E.B. Wang. *J. Coord. Chem.*, **66**, 1228 (2013).
[13] I.S. Tidmarsh, R.H. Laye, P.R. Brearley, M. Shanmugam, E.C. Sañudo, L. Sorace, A. Caneschi, E.J.L. McInnes. *Chem. Commun.*, **42**, 2560 (2006).
[14] Y. Hayashi. *Coord. Chem. Rev.*, **255**, 2270 (2011).
[15] D.C. Crans, J.J. Smee, E. Gaidamauskas, L. Yang. *Chem. Rev.*, **104**, 849 (2004).
[16] A. Müller, R. Rohlfing, A.L. Barra, D. Gatteschi. *Adv. Mater.*, **5**, 915 (1993).
[17] V. Soghomonian, Q. Chen, R.C. Haushalter, J. Zubieta, C.J. O'Connor. *Science*, **259**, 1596 (1993).
[18] L.M. Zheng, T. Whitfield, X.Q. Wang, A.J. Jacobson. *Angew. Chem. Int. Ed.*, **39**, 4528 (2000).
[19] F.B. Xin, M.T. Pope. *J. Am. Chem. Soc.*, **118**, 7731 (1996).
[20] M. Inoue, T. Yamase. *Bull. Chem. Soc. Jpn.*, **69**, 2863 (1996).
[21] D.-L. Long, P. Kögerler, L.J. Farrugia, L. Cronin. *Chem. Asian J.*, **1**, 352 (2006).
[22] U. Kortz, M.G. Savelieff, F.Y.A. Ghali, L.M. Khalil, S.A. Maalouf, D.I. Sinno. *Angew. Chem. Int. Ed.*, **41**, 4070 (2002).
[23] X.K. Fang, T.M. Anderson, C.L. Hill. *Angew. Chem. Int. Ed.*, **44**, 3540 (2005).
[24] Y. Hou, X.K. Fang, C.L. Hill. *Chem. Eur. J.*, **13**, 9442 (2007).
[25] H. Tan, Y. Li, Z. Zhang, C. Qin, X. Wang, E. Wang, Z. Su. *J. Am. Chem. Soc.*, **129**, 10066 (2007).
[26] X.L. Wang, C. Qin, E.B. Wang, Z.M. Su, Y.G. Li, L. Xu. *Angew. Chem. Int. Ed.*, **45**, 7411 (2006).
[27] D. Riou, G. Férey. *J. Solid State Chem.*, **124**, 151 (1996).
[28] S.X. Liu, B.Z. Lin, S. Lin. *Inorg. Chim. Acta*, **304**, 33 (2000).
[29] L. Ulická, F. Pavelčík, K. Huml. *Acta Crystallogr., Sect. C*, **43**, 2266 (1987).
[30] A. Tripathi, T. Hughbanks, A. Clearfield. *J. Am. Chem. Soc.*, **125**, 10528 (2003).
[31] X.L. Wang, Z.H. Kang, E.B. Wang, C.W. Hu. *Mater. Lett.*, **56**, 393 (2002).